AN EXAMPLE OF MESO-SCALE MODELING OF ACIDIC SNOW OVER THE SEA OF JAPAN

Toshihiro KITADA

Department of Ecological Engineering,
Toyohashi University of Technology,
Tempaku-cho, Toyohashi 441-8580, Japan

Target for the "Comprehensive" Model Development

- the model which can correctly reproduce mass balance of various chemical species in the atmosphere with keeping adequate accuracy for calculated concentration distributions of chemical species.

One of the important problems is reliable wet deposition prediction.

- There may be two types of methods for the modeling;

(1) one considers trans-horizontal-grids transport of aqueous phase chemical species with use of partial differential equations for these species; cloud-resolving method

(2) another one completes cloud processes within each vertical column; a simplified modeling; non cloud-resolving method – RADM, CMAQ

Examples

- Cloud-Resolving Modeling
- Non Cloud-Resolving Modeling

Role of Cloud in Transport/Transformation of Trace Chemical Species

METEOROLOGICAL MODEL

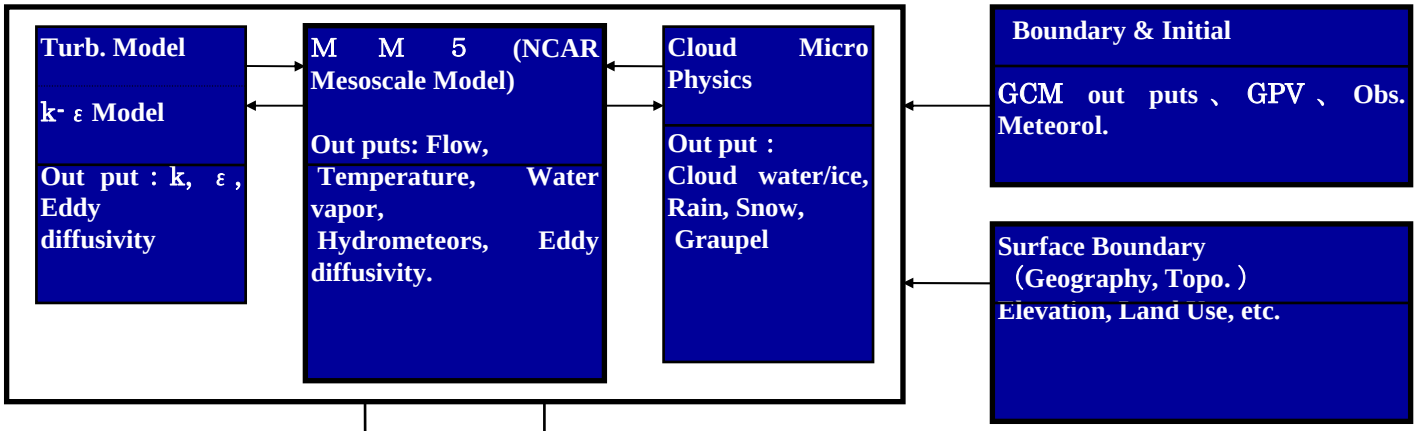

TRANPORT/CHEMISTRY/DEPOSITION MODEL

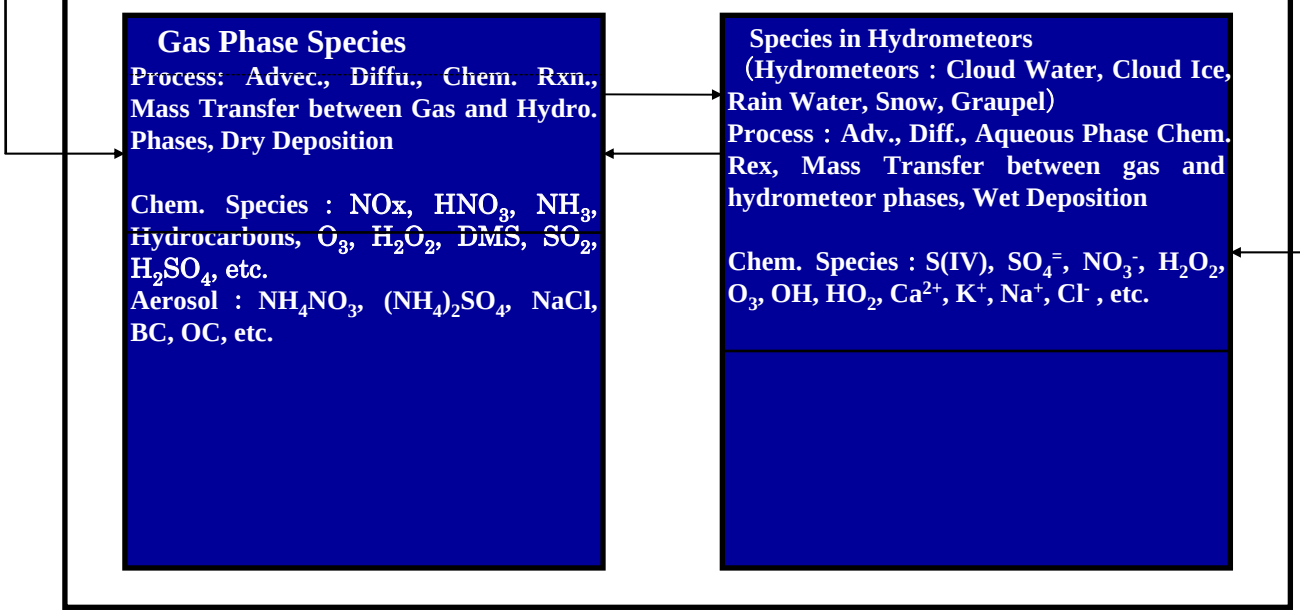

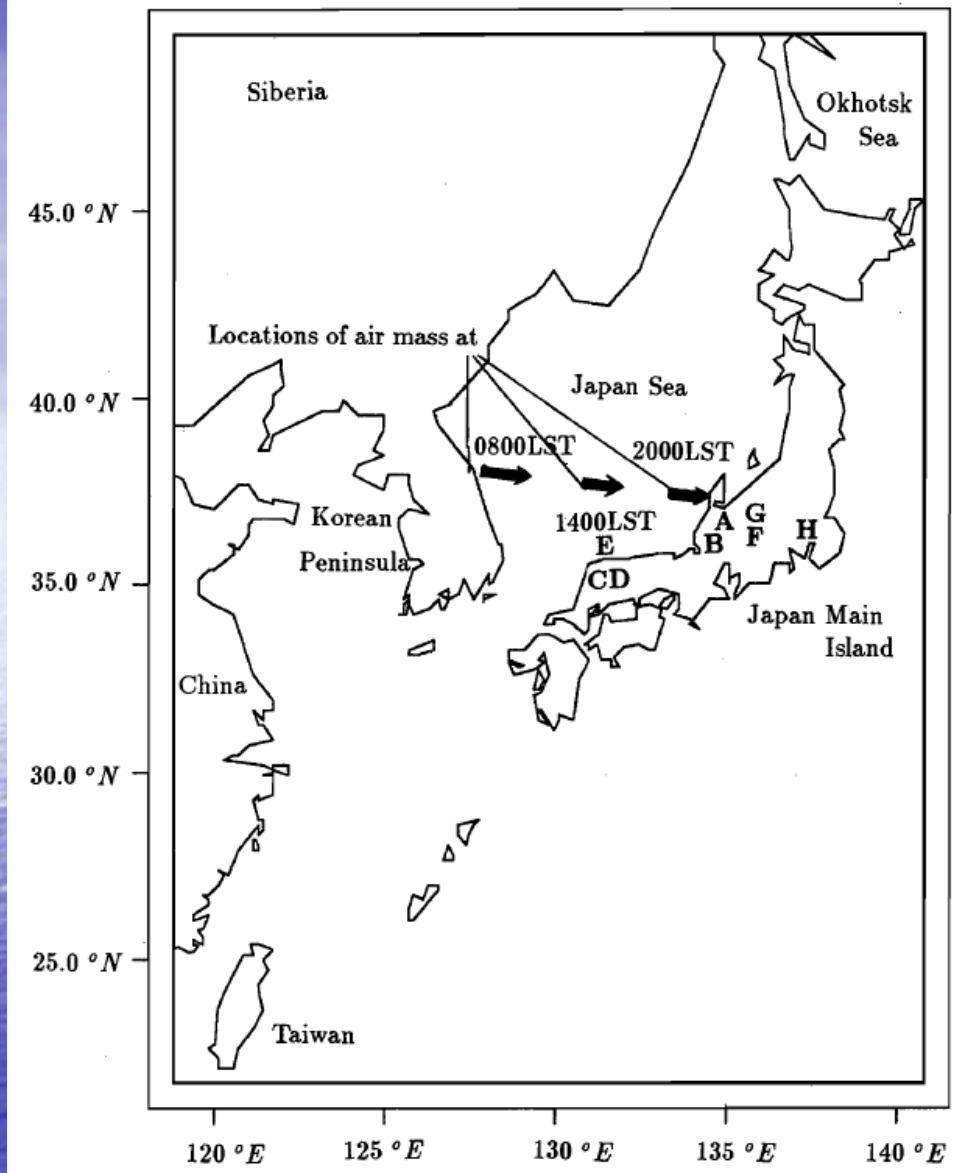

Fig. 4. The typical travelling course of the continental air mass heading over the Japan Sea in winter, which has been simulated. The locations of the air mass at 0800, 1400 and 2000 LST are indicated. The observation points of the Japanese acid snow data quoted as A–H in Section 4.4. are also marked.

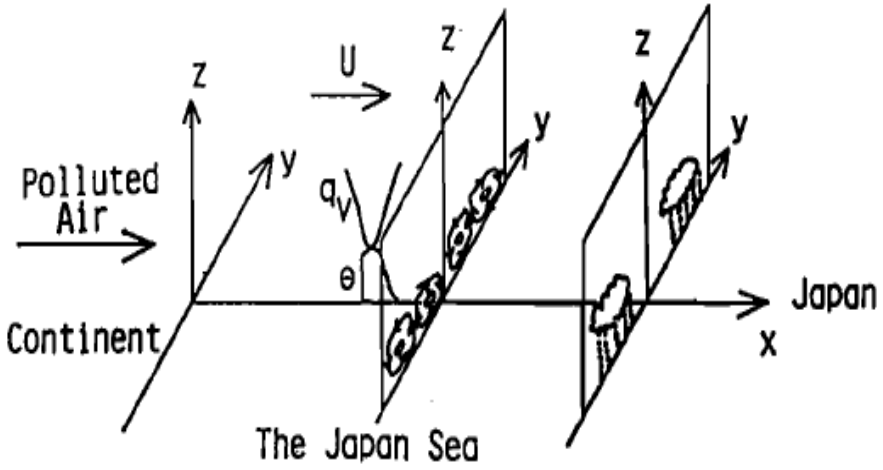

Fig. 5. Schematic diagram of the 2-D calculation domain for convective cloud streets over the Japan Sea in winter, where q_v is water vapor mixing ratio, and θ is the potential temperature.

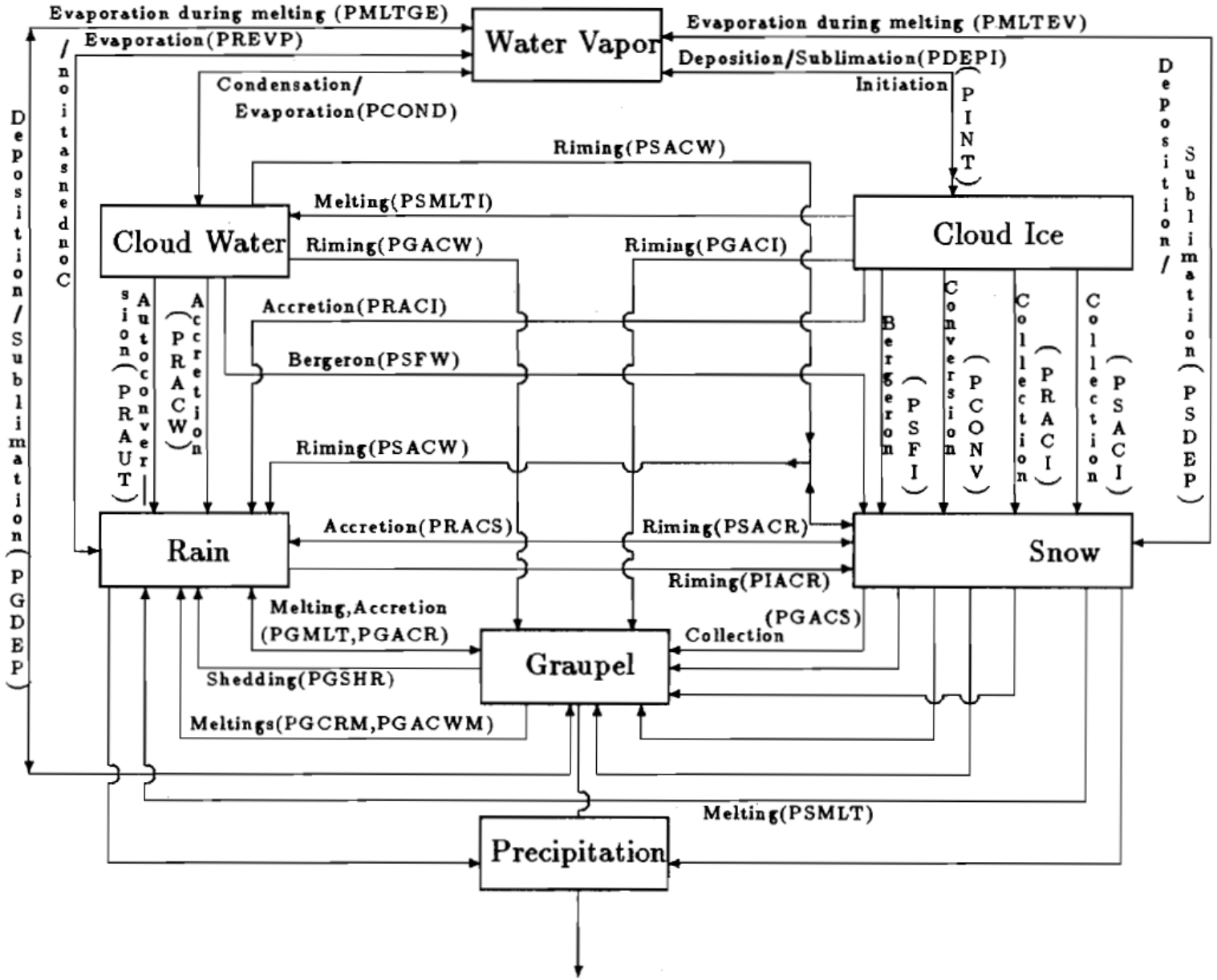

Fig. 2. Acronym diagram of inter-hydrometeor-transfers of water substance of the cloud microphysics model (after Rutledge and Hobbs, 1984).

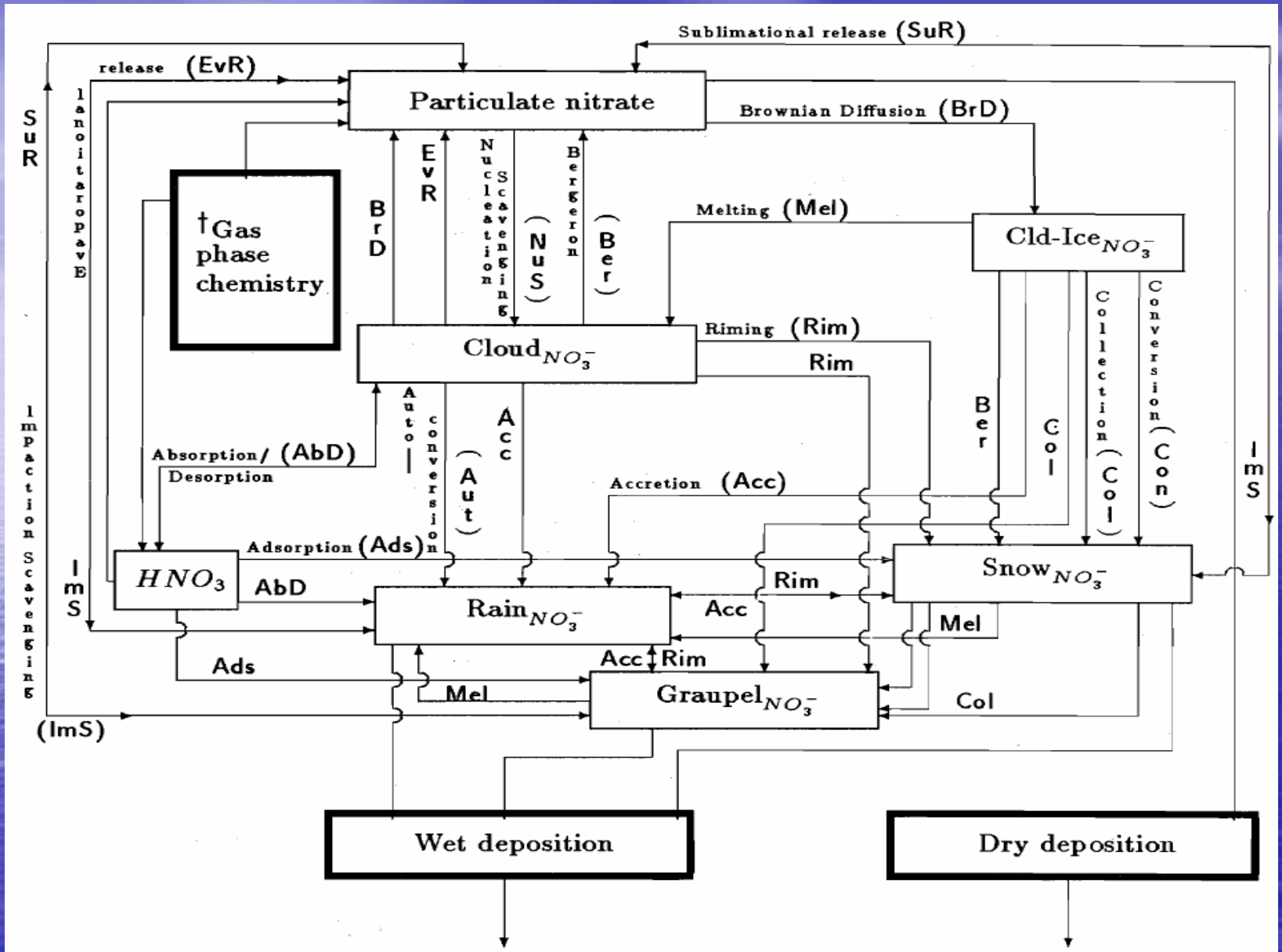

Fig. 1. Schematics showing gas–hydrometeor interphase transfers of NO_3^- adapted from Rutledge and Hobbs (1984). Normal-line boxes represent species reservoirs and thickened-line boxes represent feeding or removing processes of nitric acid and nitrate to or from these hydrometeor-phases. †The gas-phase chemistry model includes the following reactions for HNO_3 and NO_3^- productions as principal mechanisms; i.e. $NO_2+OH \rightarrow HNO_3$, $N_2O_5+H_2O \rightarrow 2HNO_3$, $NH_3+HNO_3 \Leftrightarrow NH_4NO_3$.

Table 3. Aqueous phase equilibrium reactions

	Reactions	Equilibrium constants M or M (atm.)$^{-1}$	Source
EQ1	$SO_2(g) \Leftrightarrow SO_2(aq)$	$1.23\exp[3120 \cdot f(T)^*]$	PS
EQ2	$SO_2(aq) \Leftrightarrow H^+ + HSO_3^-$	$1.23 \times 10^{-2} \exp[1960 \cdot f(T)]$	PS
EQ3	$HSO_3^- \Leftrightarrow H^+ + SO_3^{2-}$	$6.61 \times 10^{-8} \exp[1500 \cdot f(T)]$	PS
EQ4	$NH_3(g) \Leftrightarrow NH_3(aq)$	$75\exp[3400 \cdot f(T)]$	PS
EQ5	$NH_3(aq) \Leftrightarrow NH_4^+ + OH^-$	$1.75 \times 10^{-5} \exp[-450 \cdot f(T)]$	PS
EQ6	$HNO_3(g) \Leftrightarrow H^+ + NO_3^-$	$2.6 \times 10^{6} \exp[8700 \cdot f(T)]$	C
EQ7	$CO_2(g) \Leftrightarrow CO_2(aq)$	$3.4 \times 10^{-2} \exp[2420 \cdot f(T)]$	PS
EQ8	$CO_2(aq) \Leftrightarrow HCO_3^- + H^+$	$4.46 \times 10^{-7} \exp[-1000 \cdot f(T)]$	PS
EQ9	$HCO_3^- \Leftrightarrow CO_3^{2-} + H^+$	$4.68 \times 10^{-11} \exp[-1760 \cdot f(T)]$	PS
EQ10	$O_3(g) \Leftrightarrow O_3(aq)$	$1.13 \times 10^{-2} \exp[2300 \cdot f(T)]$	PS
EQ11	$H_2O_2(g) \Leftrightarrow H_2O_2(aq)$	$7.45 \times 10^{4} \exp[6620 \cdot f(T)]$	PS
EQ12	$HO_2(g) \Leftrightarrow HO_2(aq)$	$2 \times 10^{3} \exp[6640 \cdot f(T)]$	PS
EQ13	$OH(g) \Leftrightarrow OH(aq)$	$25\exp[5280 \cdot f(T)]$	PS
EQ14	$H_2O \Leftrightarrow H^+ + OH$	1×10^{14}	PS

*$f(T) \equiv \frac{1}{T} - \frac{1}{298}$ where T is temperature in K.

PS: Pandis and Seinfeld (1989).

C: Chameides (1984).

Table 4. Aqueous phase reactions

Reactions	Rates s^{-1}, $M^{-1}s^{-1}$ or $M^{-2}s^{-1}$	Source
R1 $H_2O_2 \xrightarrow{h\nu} 2\cdot OH$	1.0×10^{-6}	ES
R2 $OH + HO_2 \rightarrow H_2O + O_2$	$1.1 \times 10^{12} \exp[-1500/T]$	PS
R3 $OH + H_2O_2 \rightarrow H_2O + HO_2$	$8.1 \times 10^{9} \exp[-1700/T]$	PS
R4 $HO_2 + HO_2 \rightarrow H_2O_2 + O_2$	$2.4 \times 10^{9} \exp[-2365/T]$	PS
R5 $S(IV) + O_3 \rightarrow S(VI) + O_2$	for $SO_2(aq)$: 2.4×10^{4}	
	for HSO_3^-: $4.2 \times 10^{13} \exp[-5530/T]$	
	for SO_3^{2-}: $7.4 \times 10^{16} \exp[-5280/T]$	PS
R6 $S(IV) + H_2O_2 \rightarrow S(VI) + H_2O$	$3.7 \times 10^{12} \exp[-4430/T]$	PS
R7 $S(IV) + \frac{1}{2}\cdot O_2 \xrightarrow{Fe^{3+},\, Mn^{2+}} S(VI)$	*	M

* $pH \leqslant 5$: $$-4.6 \times 10^{23} \exp\left[-\frac{13{,}700}{T}\right][Mn^{2+}][HSO_3^-]$$
$$-8.8 \times 10^{15} \exp\left[-\frac{11{,}000}{T}\right][Fe^{3+}]\left(\frac{[SO_2(aq)] + [HSO_3^-]}{[H^+]}\right).$$

$pH > 5$: $$-4.6 \times 10^{23} \exp\left[-\frac{13{,}700}{T}\right][Mn^{2+}][HSO_3^-].$$

PS: Pandis and Seinfeld (1989).
M: Martin (1984).
ES: estimated for noon time in Jan. at 40°N.

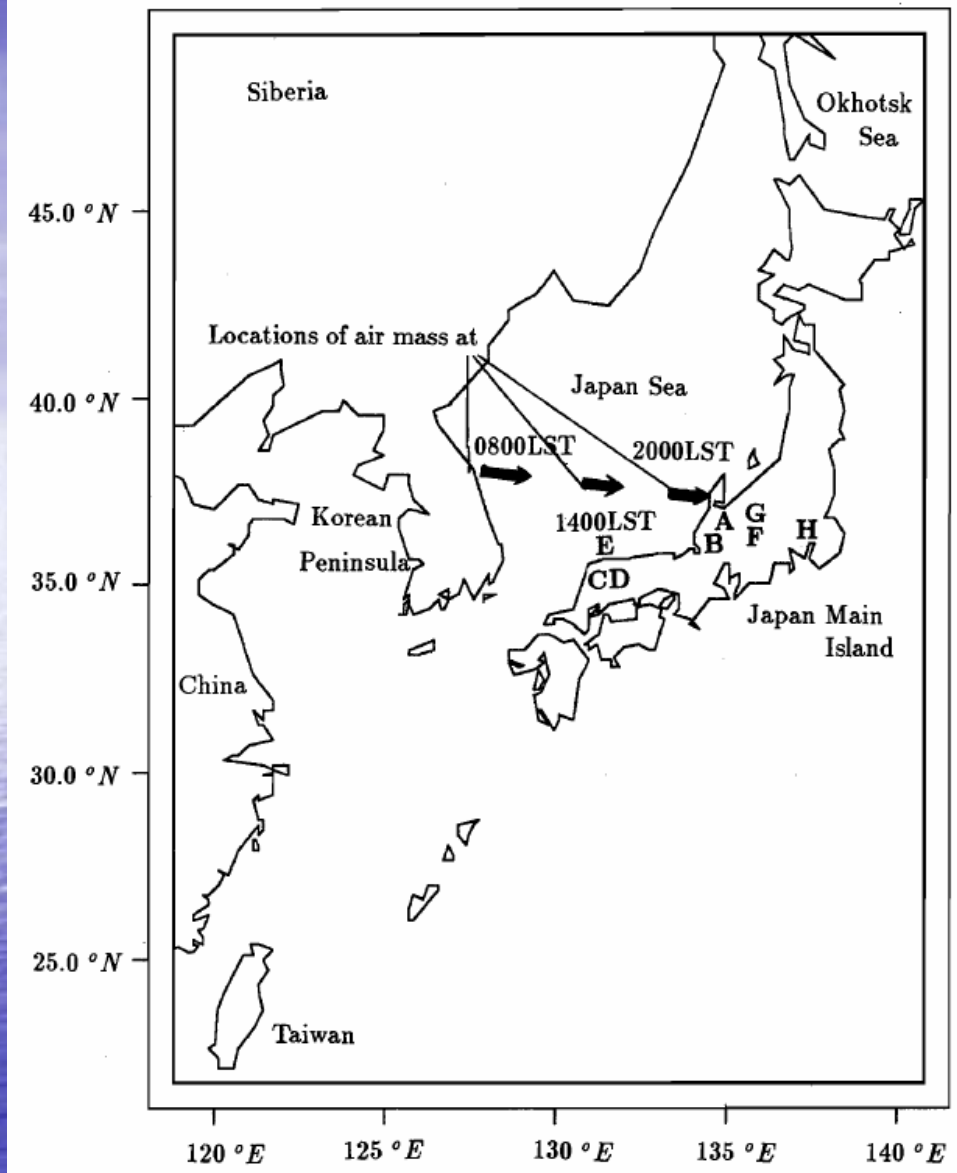

Fig. 4. The typical travelling course of the continental air mass heading over the Japan Sea in winter, which has been simulated. The locations of the air mass at 0800, 1400 and 2000 LST are indicated. The observation points of the Japanese acid snow data quoted as A–H in Section 4.4. are also marked.

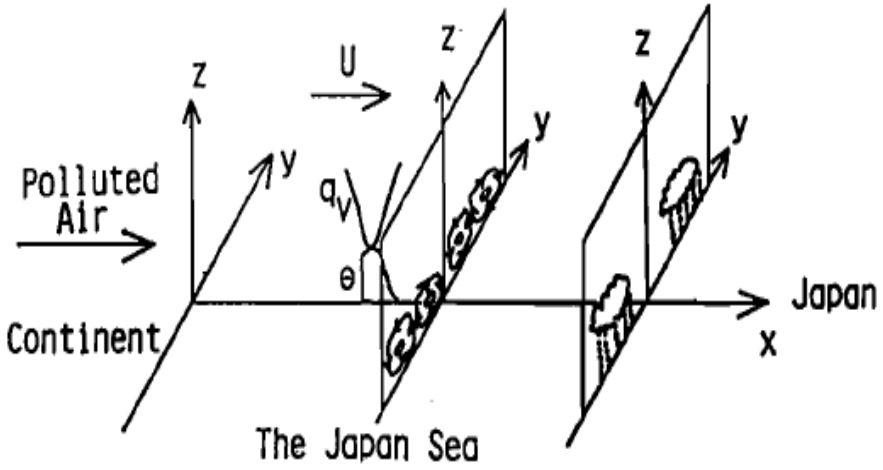

Fig. 5. Schematic diagram of the 2-D calculation domain for convective cloud streets over the Japan Sea in winter, where q_v is water vapor mixing ratio, and θ is the potential temperature.

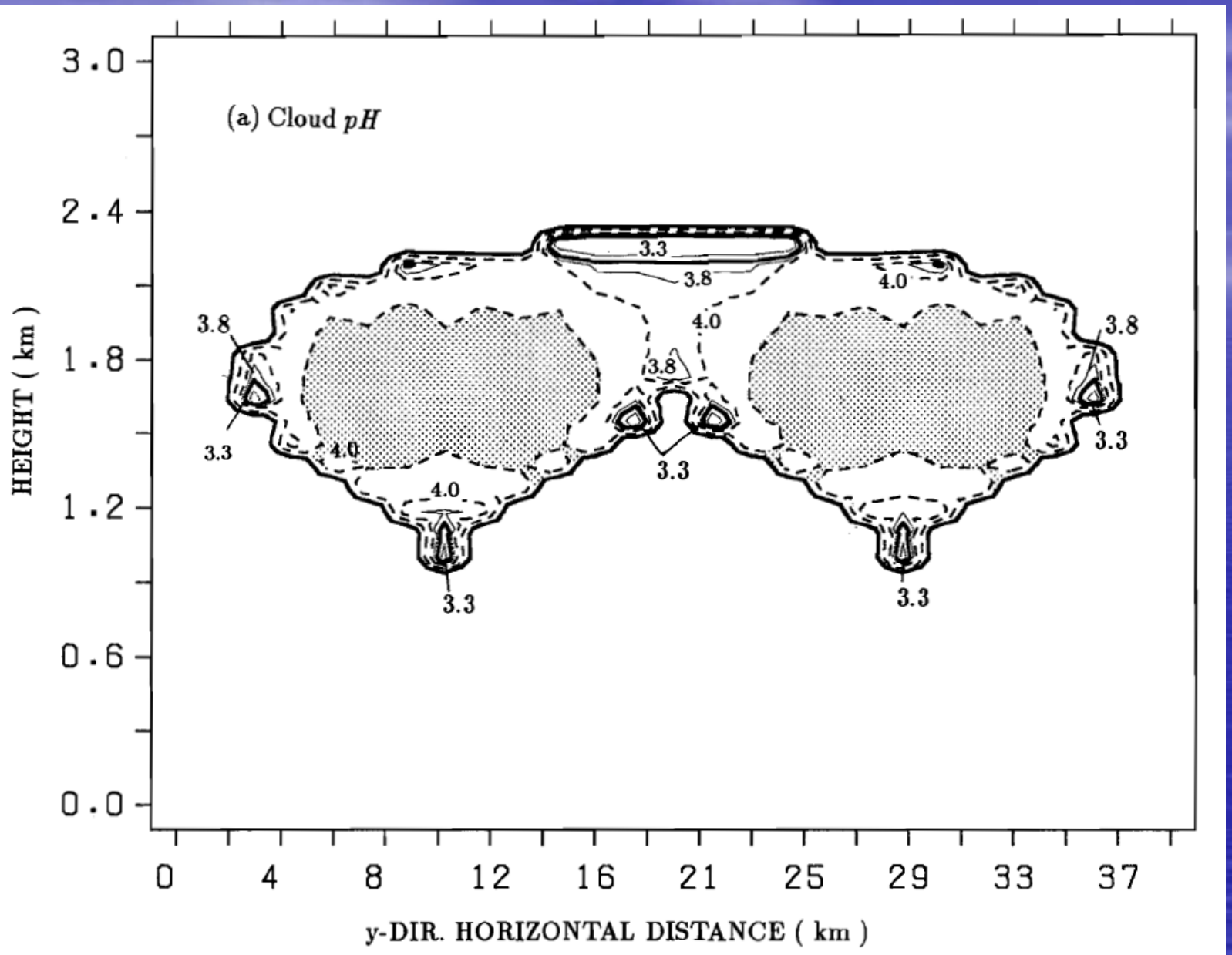

Fig. 4. Predicted contour maps of (a) cloud pH (stippling for pH > 4.4), and (b) cloud NO_3^- (stippling for concentration > 5) and (c) cloud SO_4^{2-} (stippling for concentration > 3) at 2000 LST, in nmole kg-air^{-1}.

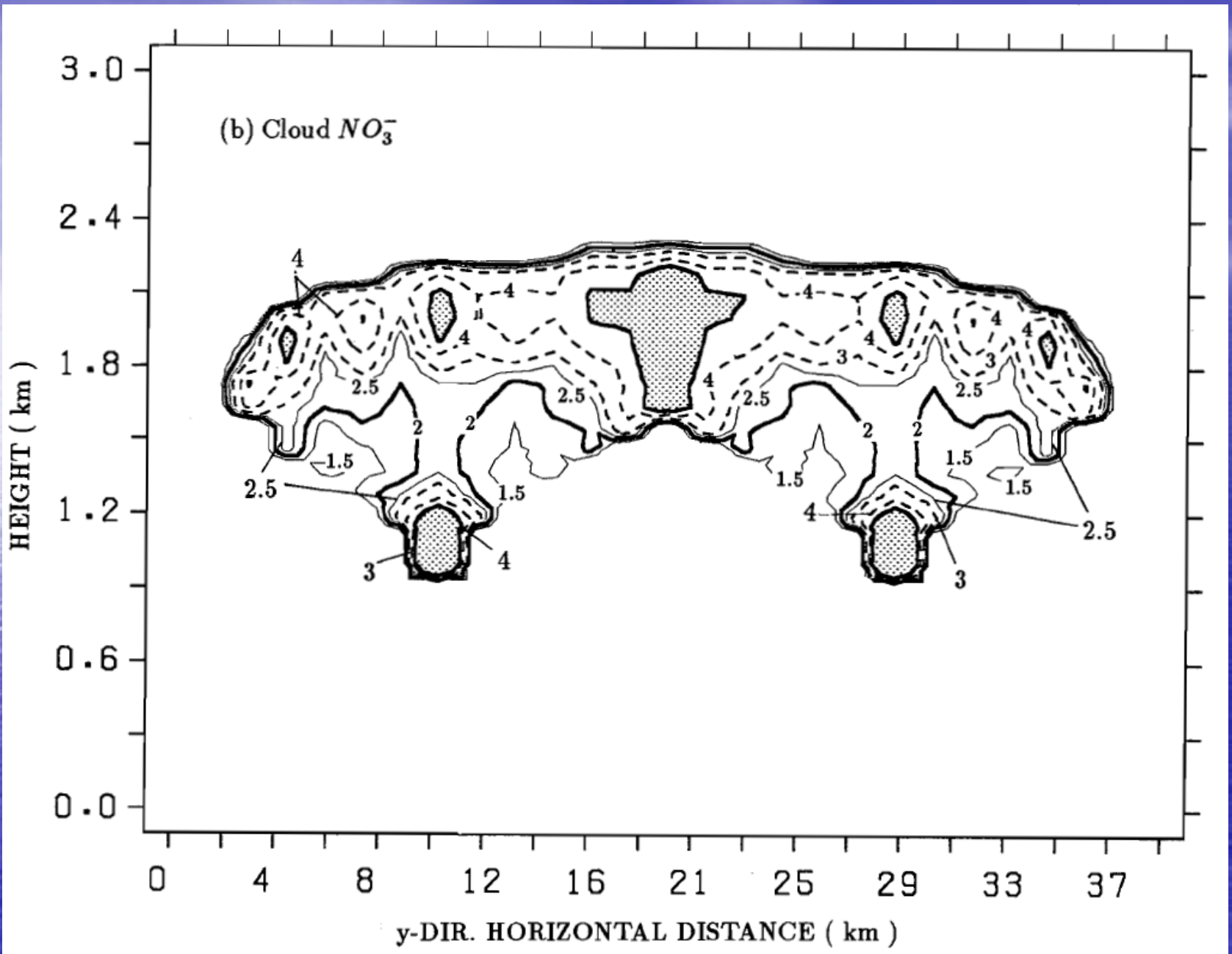

Fig. 4. (Continued)

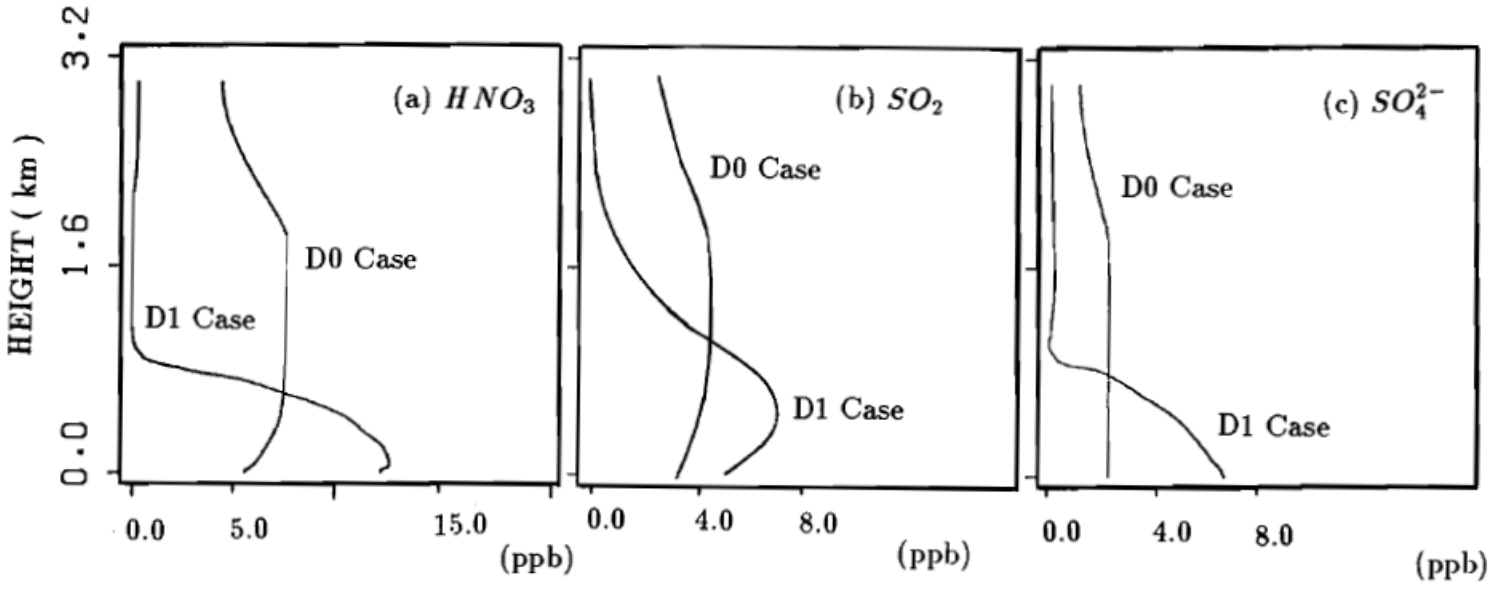

Fig. 1. Comparison of predicted vertical profiles of gas-phase concentrations (ppb), between D0 (no-cloud) and D1 (with-cloud) cases: (a) HNO_3, (b) SO_2 and (c) SO_4^{2-} at 2000 LST along $y|_{\text{max, updraft}} = 10.5$ km.

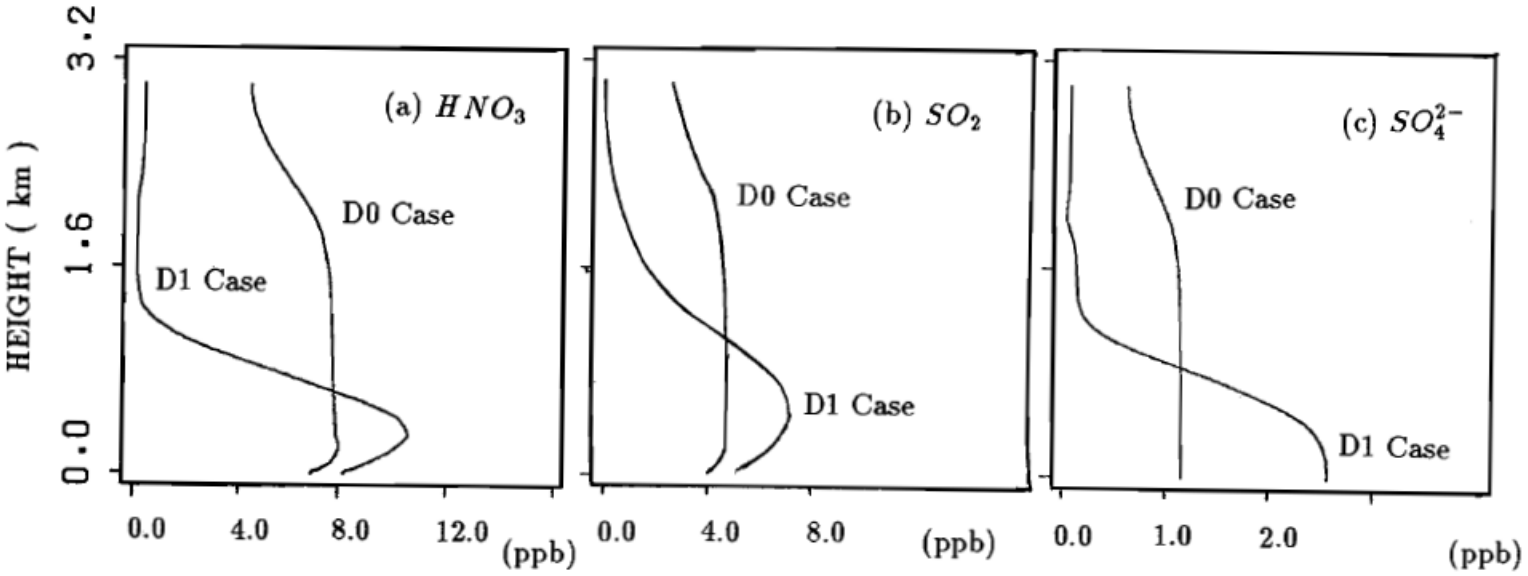

Fig. 2. Same as in Fig. 1, but for $y|_{\text{max, downdraft}} = 19.5$ km.

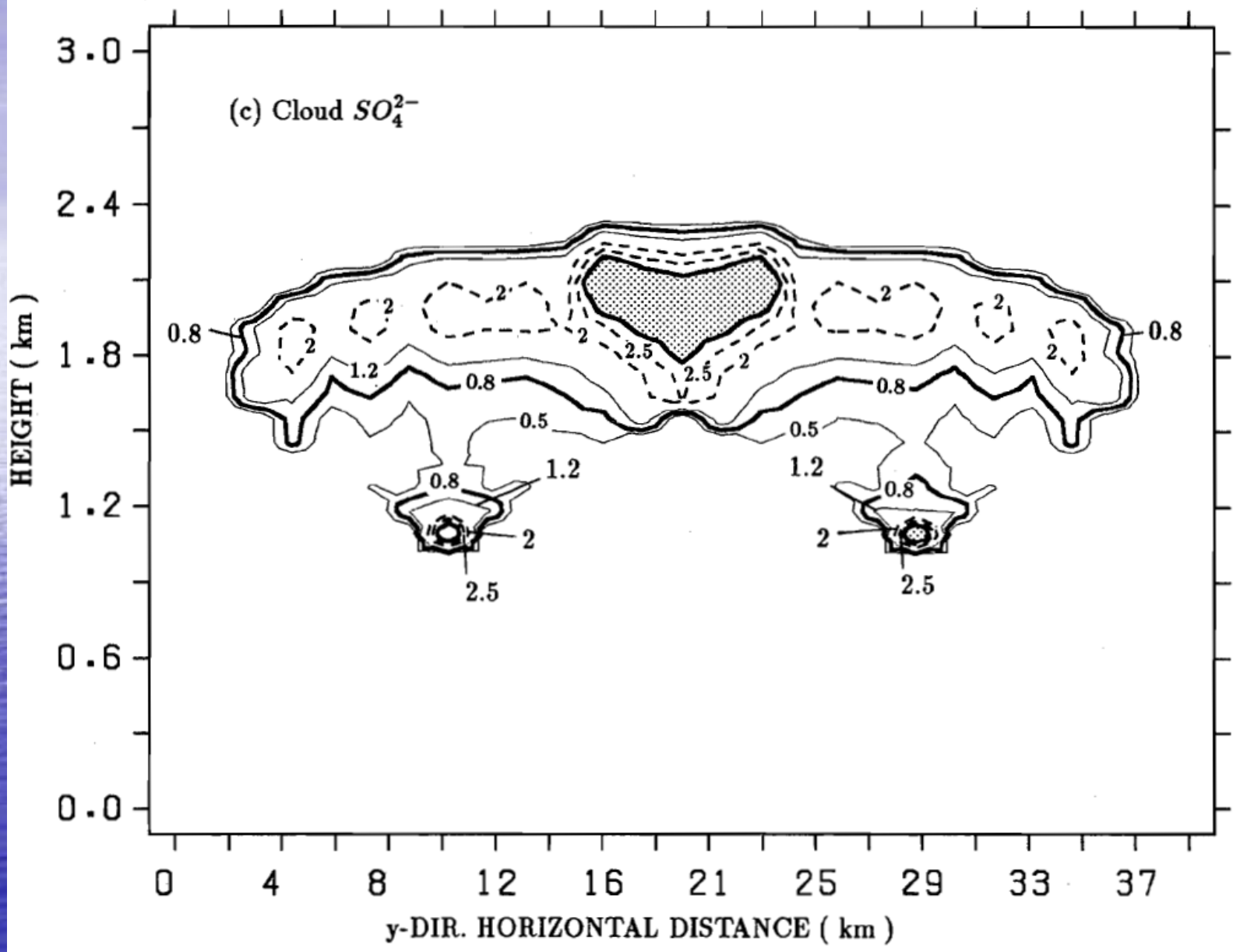

Fig. 4. (Continued)

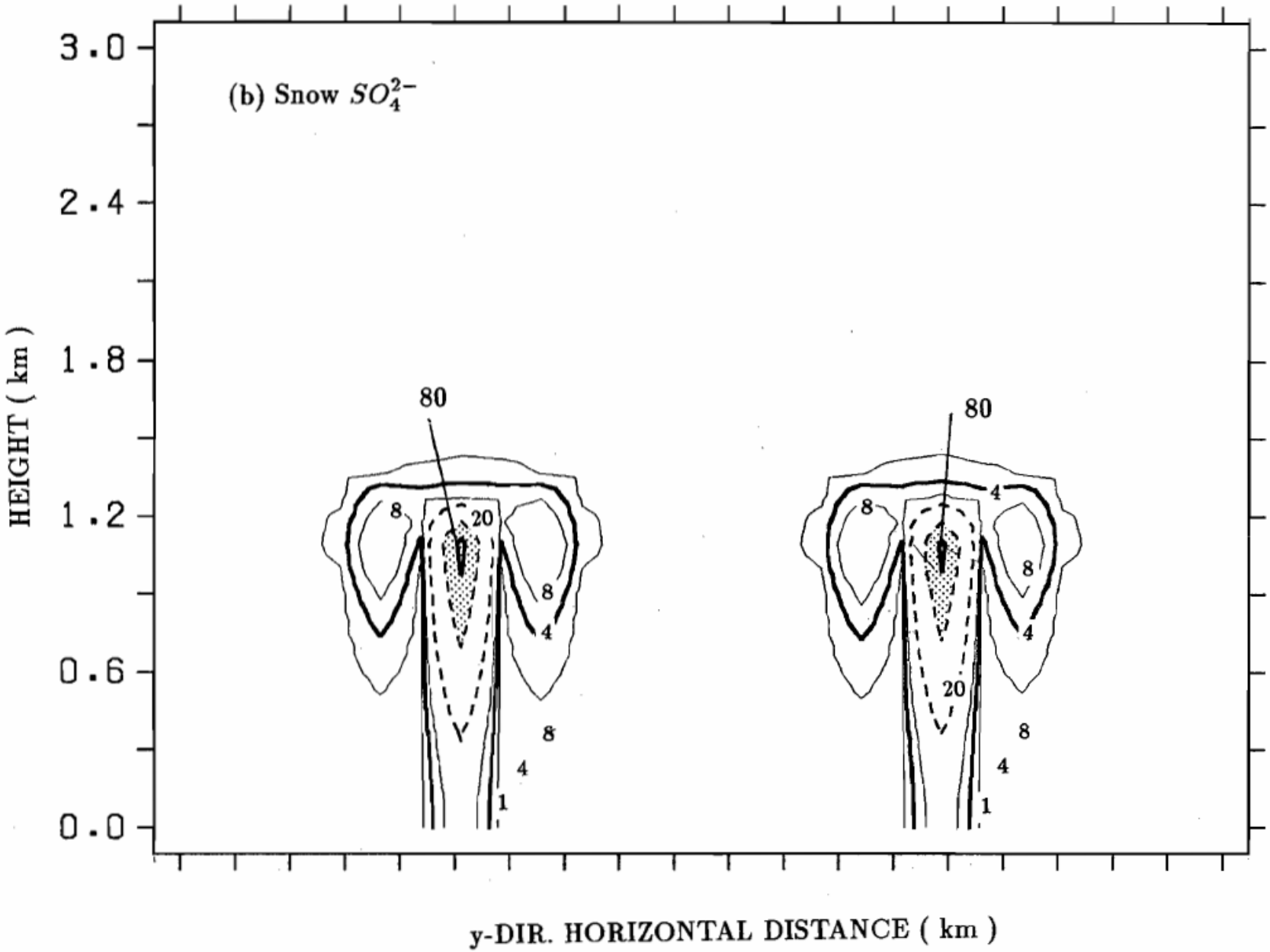

Fig. 6. (Continued)

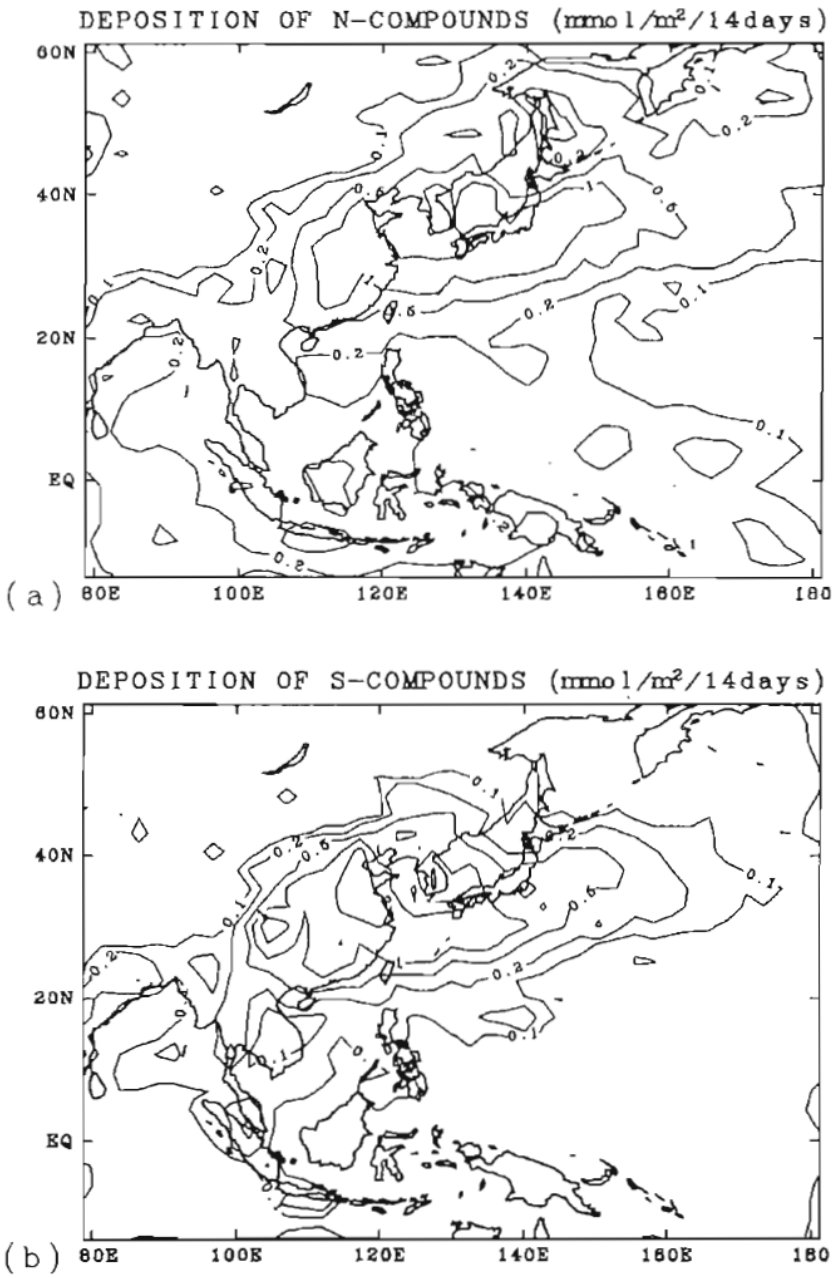

Figure 5. Calculated dry + wet deposition (BASE) of (a) N- and (b) S-compounds in mmol m^{-2} $(14day)^{-1}$. The fourteen day stands for the period from 00GMT, 1 March to 00GMT, 15 March, 1994. Contour lines : 0.1, 0.2, 0.5, 1, and 2.

Observation Point in China

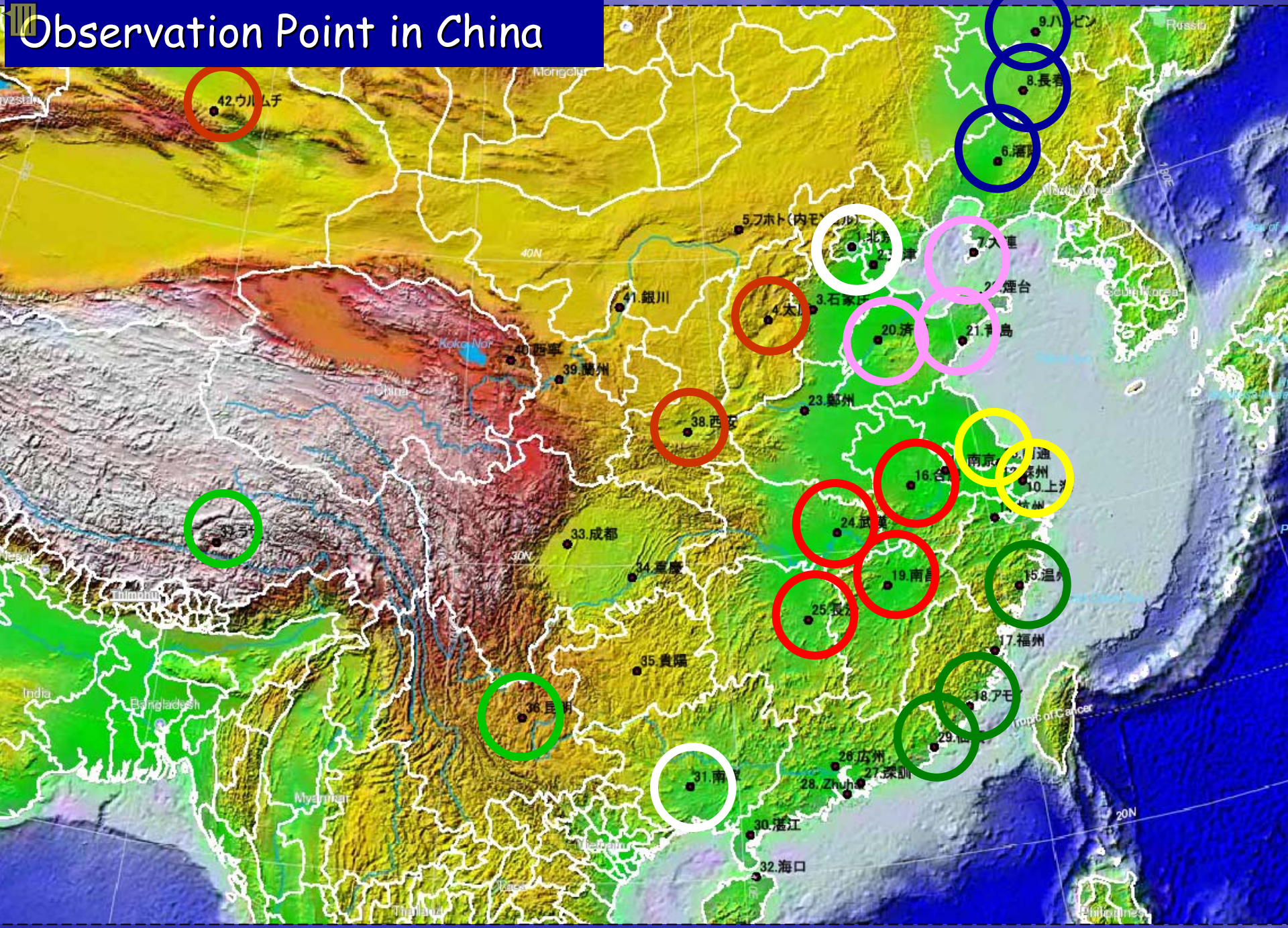

Below top of cloud layer: scavenging of gas/aerosol phase species by hydrometeors,

$$\frac{\partial CX_i}{\partial t} = -\Lambda CX_i \tag{9}$$

For rain,

$$\Lambda_{p,rain} = 6 \times 10^{-4} \eta_r P^{0.75} \tag{2}$$

where $\Lambda_{p,rain}$ denotes the scavenging coefficient for particle due to rain in s^{-1}, η_r the collection efficiency of aerosol by rain and was assumed to be $0.3 \sim 0.5$, and P the precipitation intensity in $mmhr^{-1}$.

For snow, following Slinn (1974),

$$\Lambda_{p,snow} = \frac{\rho_w g \eta_s (3.6 \times 10^{-6} P)}{\rho_a V_t^2} \tag{3}$$

where ρ_w denotes the density of water ($= 1000$ kgm^{-3}), g the gravitational acceralation ($= 9.8$ ms^{-2}), ρ_a the air density (~ 1 kg m^{-3}), V_t the average settling velocity of the snow flakes in ms^{-1} and is expressed by the following equation recommended by Knutson *et al.* (1976):

$$V_t = (102 + 51 \log_{10} d_c)/100 \tag{4}$$

where d_c denotes the diameter of the circle circumscribed about the average snowflake in cm. $\Lambda_{p,snow}$ in Eq.(3) was approximated as 5.6×10^{-4}P by assuming d_c=500μm and η_s=0.002 (judged from figure in Slinn, 1977).

Coefficients (s^{-1}) for scavenging, due to rain, of gaseous species were given in the model, for example, for SO_2;

$$\Lambda_{SO2} = \beta \frac{\alpha P}{3.6H} \tag{5}$$

$$\alpha = 10^{-6} RT H_{eff,SO_2} \tag{6}$$

where H denotes the height of cloud-top in m, R the universal gas constant (=0.082ℓ atm K^{-1} mol^{-1}), T the air temperature in K, and H_{eff,SO_2} the inverse of the effective Henry's law

constant for SO_2 in mole ℓ^{-1} atm^{-1}, which is a function of the hydrogen ion concentration in rain drop, and is defined as:

$$H_{eff,SO_2} = K_1 \left(1 + \frac{K_2}{[H^+]} + \frac{K_2 K_3}{[H^+]^2} \right) \tag{7}$$

where K_1, K_2, and K_3 are equilibrium constants of the following reactions with concentrations in atm and M:

$$SO_2(g) \rightleftharpoons SO_2(\ell) \; : \; K_1 = 1.23 \exp\left[3120 \left(\frac{1}{T} - \frac{1}{298}\right)\right]$$

$$SO_2(\ell) \rightleftharpoons H^+ + HSO_3^- \; : \; K_2 = 1.23 \times 10^{-2} \exp\left[1960 \left(\frac{1}{T} - \frac{1}{298}\right)\right]$$

$$HSO_3^- \rightleftharpoons H^+ + SO_3^{2-} \; : \; K_3 = 6.61 \times 10^{-8} \exp\left[1500 \left(\frac{1}{T} - \frac{1}{298}\right)\right]$$

For absorption of HNO_3,

$$H_{eff,HNO_3} = \frac{K_4}{[H^+]} \tag{8}$$

where K_4 denotes equilibrium constant for

$$HNO_3(g) \rightleftharpoons H^+ + NO_3^- \; : \; K_4 = 2.6 \times 10^6 \exp\left[8700 \left(\frac{1}{T} - \frac{1}{298}\right)\right]$$

constant for SO_2 in mole ℓ^{-1} atm^{-1}, which is a function of the hydrogen ion concentration in rain drop, and is defined as:

$$H_{eff,SO_2} = K_1 \left(1 + \frac{K_2}{[H^+]} + \frac{K_2 K_3}{[H^+]^2} \right) \tag{7}$$

where K_1, K_2, and K_3 are equilibrium constants of the following reactions with concentrations in atm and M:

$$SO_2(g) \rightleftharpoons SO_2(\ell) \; : \; K_1 = 1.23 \exp\left[3120 \left(\frac{1}{T} - \frac{1}{298}\right)\right]$$

$$SO_2(\ell) \rightleftharpoons H^+ + HSO_3^- \; : \; K_2 = 1.23 \times 10^{-2} \exp\left[1960 \left(\frac{1}{T} - \frac{1}{298}\right)\right]$$

$$HSO_3^- \rightleftharpoons H^+ + SO_3^{2-} \; : \; K_3 = 6.61 \times 10^{-8} \exp\left[1500 \left(\frac{1}{T} - \frac{1}{298}\right)\right]$$

For absorption of HNO_3,

$$H_{eff,HNO_3} = \frac{K_4}{[H^+]} \tag{8}$$

where K_4 denotes equilibrium constant for

$$HNO_3(g) \rightleftharpoons H^+ + NO_3^- \; : \; K_4 = 2.6 \times 10^6 \exp\left[8700 \left(\frac{1}{T} - \frac{1}{298}\right)\right]$$

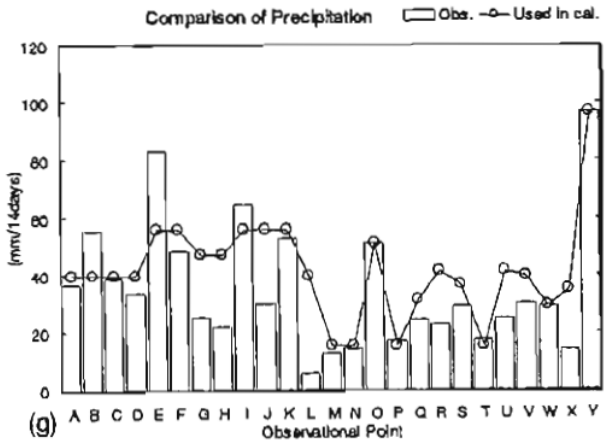

Figure 8. (Continued)

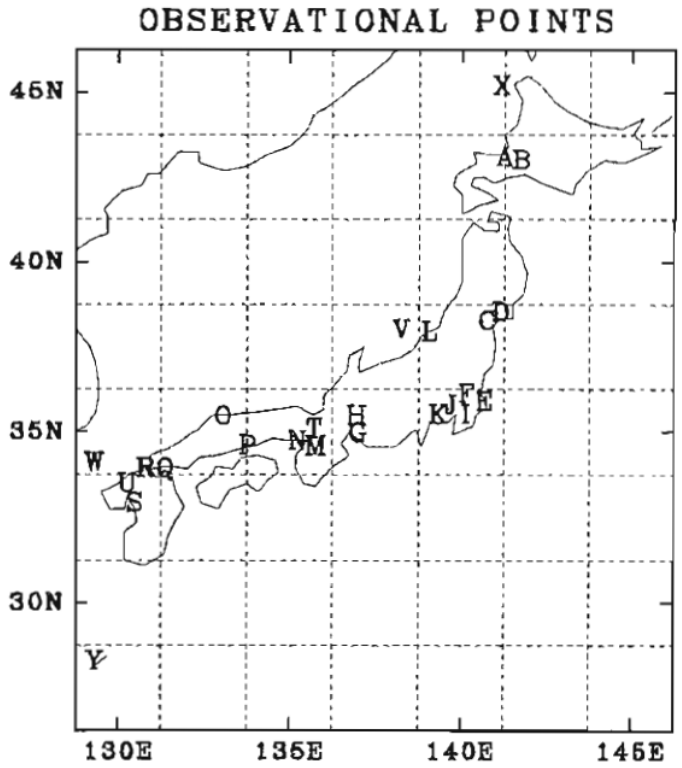

Figure 9. Observation points for acid deposition : points A through Y. One grid cell written with dashed lines expresses area of 2.5 °× 2.5 °. See also caption for Fig. 8.

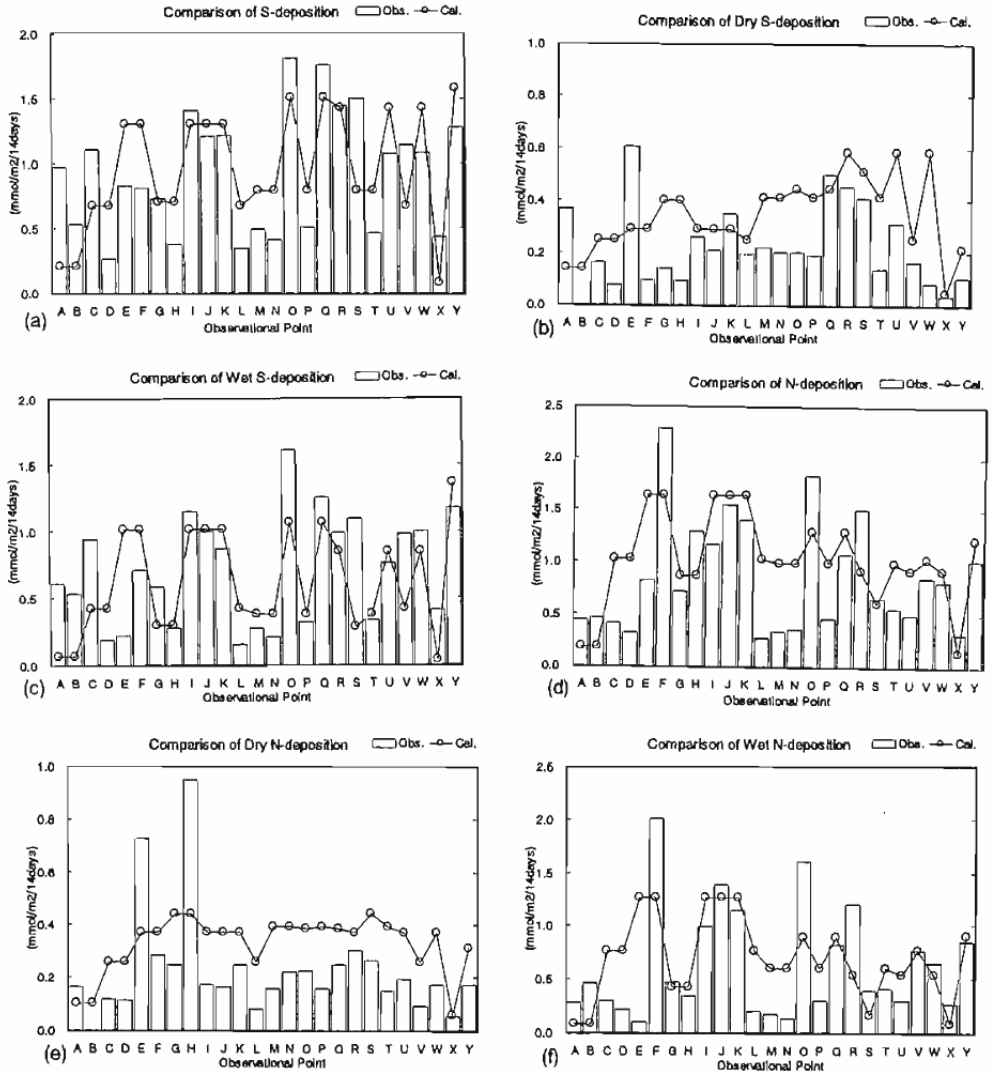

Figure 8. Comparison of the calculated deposition (BASE) with the observed at 25 points in Japan : (a) S-total-, (b) S-dry-, and (c) S-wet-depositions, where S-compounds denote SO_2 and SO_4^{2-} ; (d) N-total-, (e) N-dry-, (f) N-wet-depositions, where N-compound means HNO_3 (NO_3^-) : Fig. 8(g) shows precipitation : the observation with bar graph and the data (Xie and Arkin, 1995) used in the present simulation. Observation points : A-Sapporo, B-Nohoro, C-Sendai, D-Eno-dake, E-Kashima, F-Tsukuba, G-Nagoya, H-Inuyama, I-Ichihara, J-Tokyo, K-Kawasaki, L-Niigata, M-Osaka, N-Amagasaki, O-Matsue, P-Kurashiki, Q-Ube, R-Kitakyusyu, S-Omuta, T-Kyoto-Hachiman, U-Chikugo-Ogori, V-Sado, W-Tsushima, X-Rishiri, and Y-Amami. The locations of these points are shown in Fig. 9.

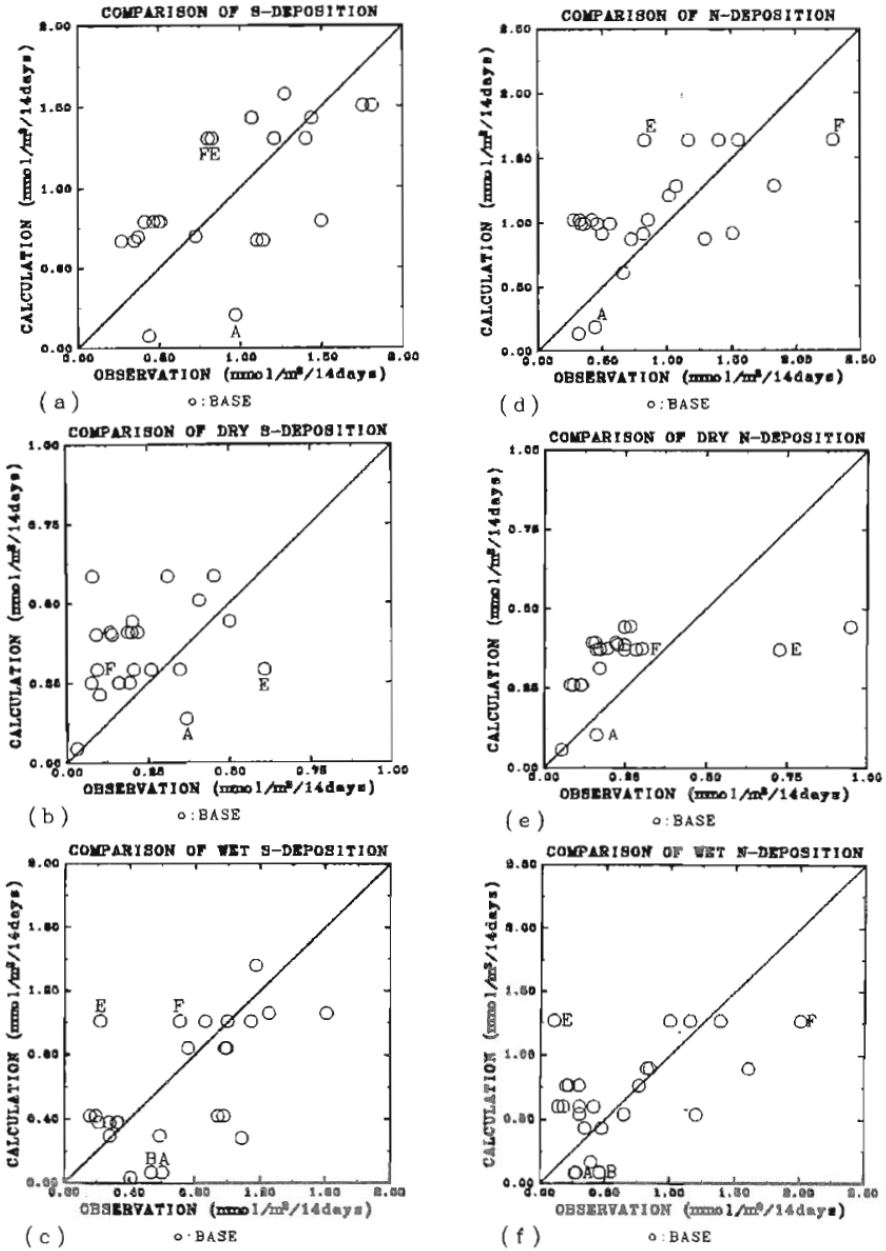

Figure 10. Calculated(BASE in Table 2) VS. observed depositions at the points A through Y in Fig. 9 : (a) S-total-, (b) S-dry-, and (c) S-wet-depositions ; similarly (d) N-total-, (e) N-dry-, and (f) N-wet-depositions. The N-wet-deposition includes that of HNO_3 (NO_3^-). The letter A indicates Sapporo, B Nohoro, E Kashima and F Tsukuba. At Nohoro (i.e. B), only wet-deposition was observed.

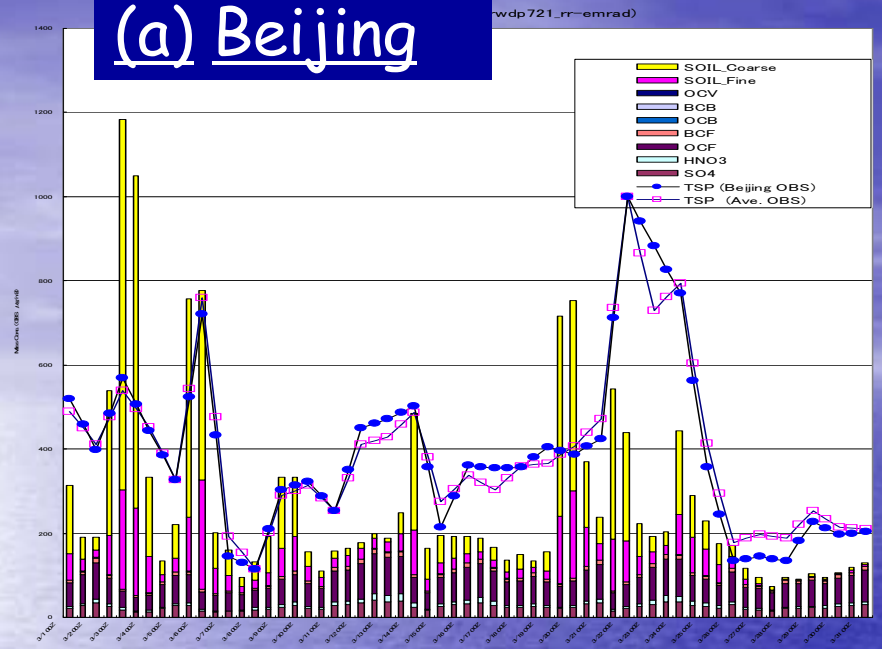

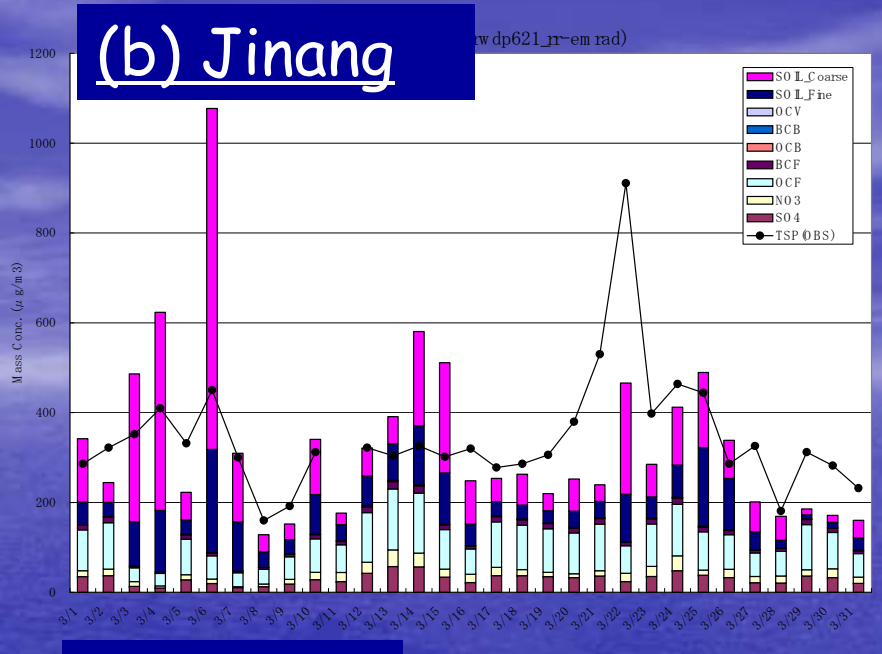

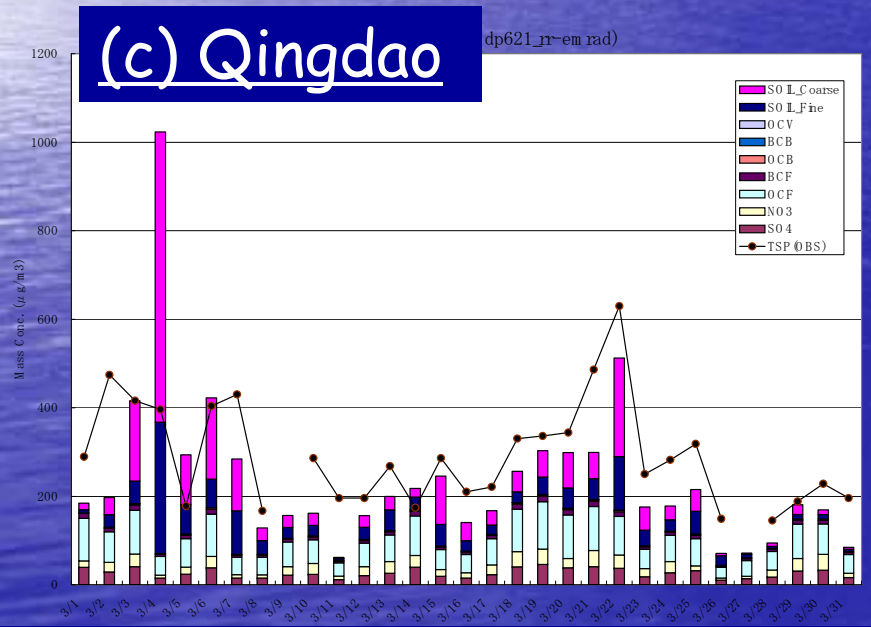

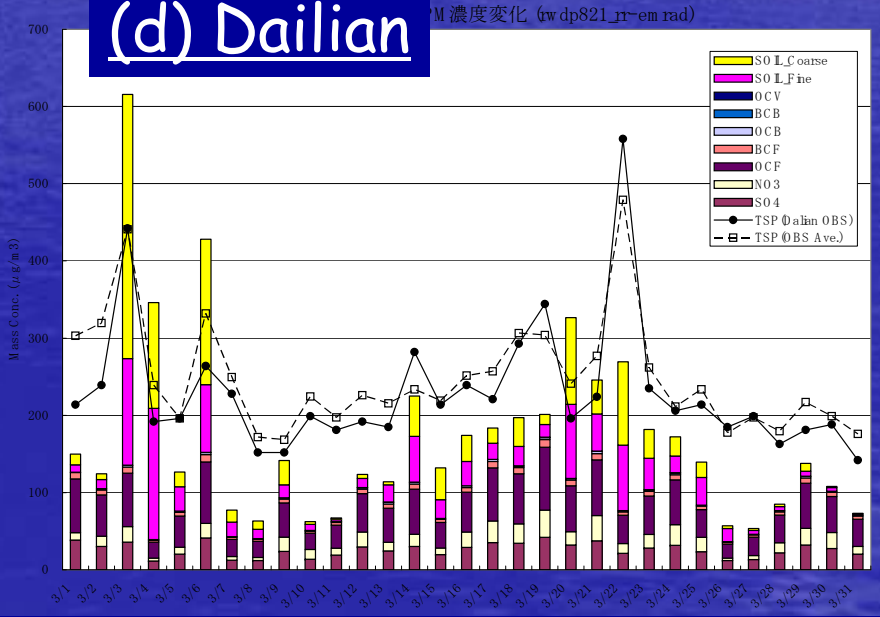

Beijing & South or East of Beijing: 北京、斉南、青島、大連

(a) KUNMING

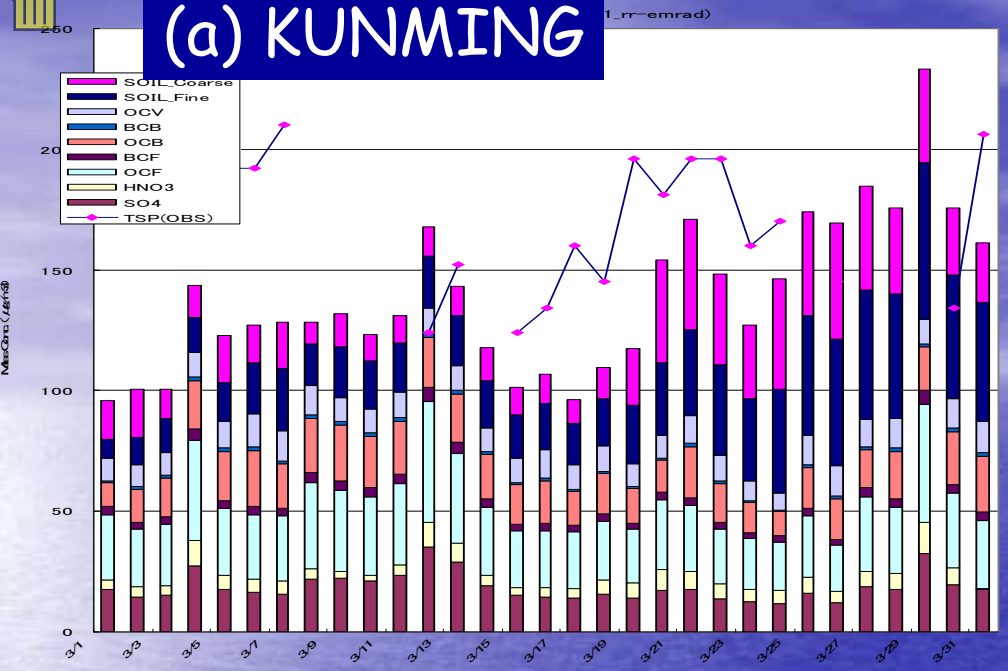

Southeastern Mountainous Area: Kunming(昆明)

(b) LHASA

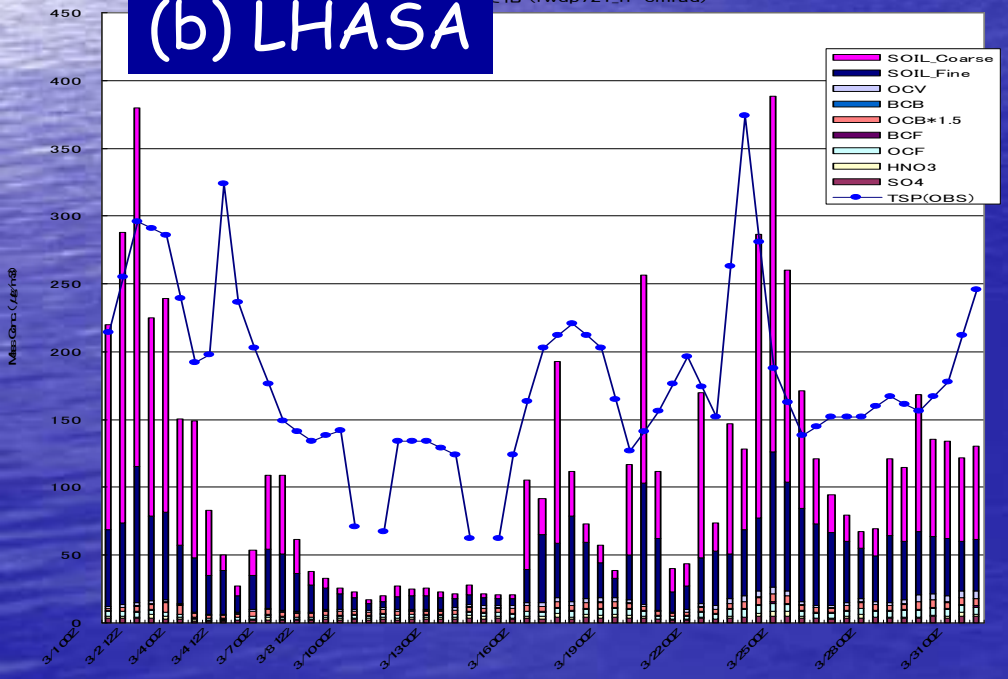

Southern Highland Area (Tibet): Lhasa(ラサ)

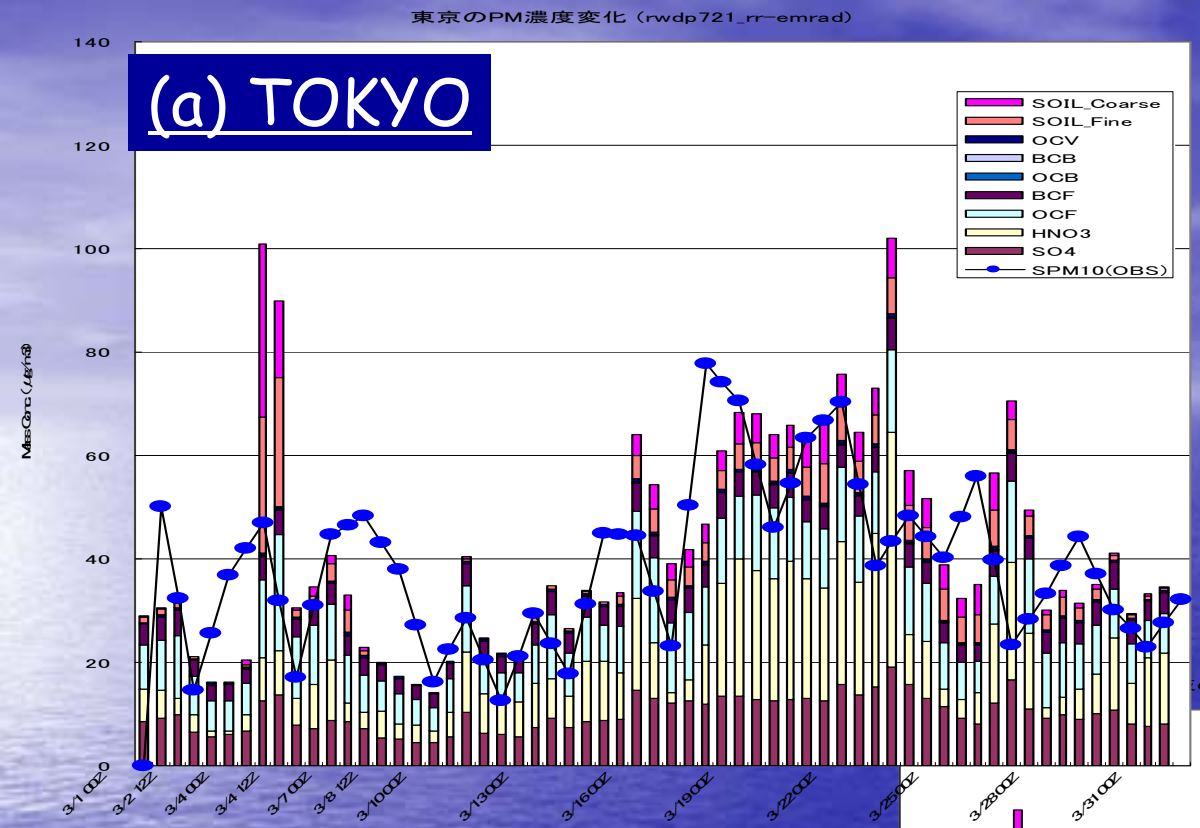
東京のPM濃度変化（rwdp721_rr-emrad）
(a) TOKYO
SOIL_Coarse
SOIL_Fine
OCV
BCB
OCB
BCF
OCF
HNO3
SO4
SPM10(OBS)
140
120
100
80
60
40
20
0
3/1 0Z
3/2 12Z
3/4 0Z
3/4 12Z
3/7 0Z
3/8 12Z
3/10 0Z
3/13 0Z
3/16 0Z
3/19 0Z
3/22 0Z
3/25 0Z
3/28 0Z
3/31 0Z

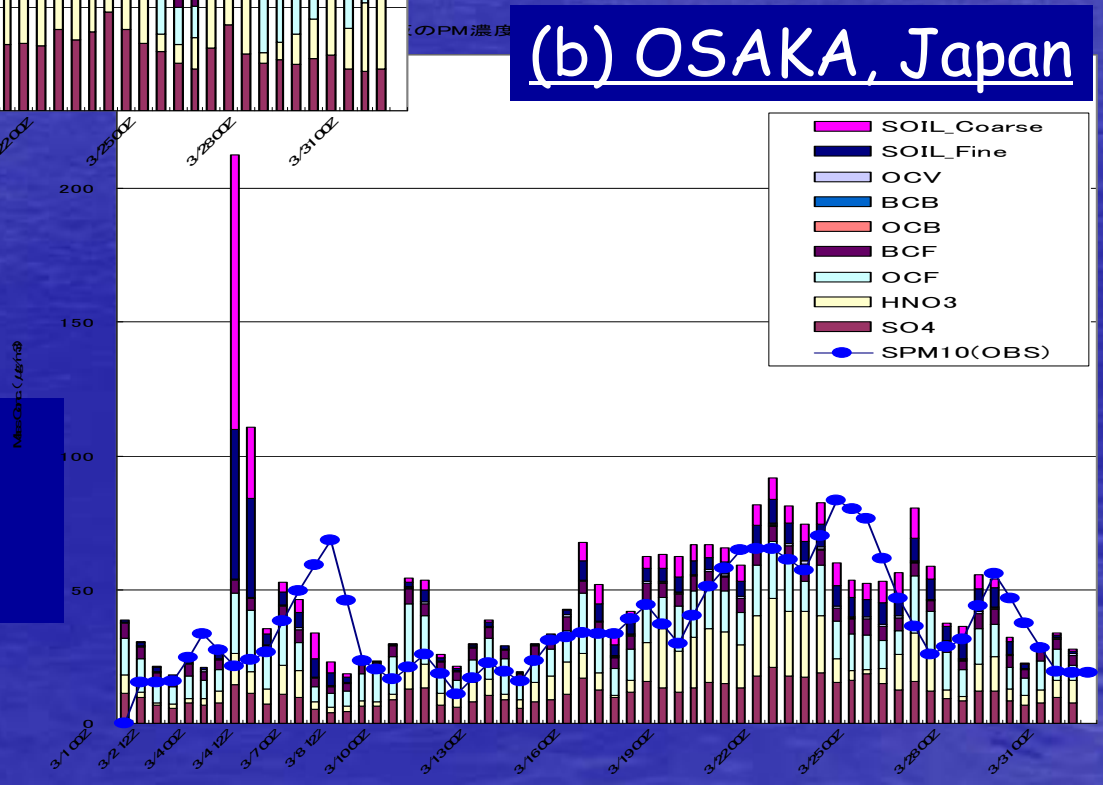
(b) OSAKA, Japan
SOIL_Coarse
SOIL_Fine
OCV
BCB
OCB
BCF
OCF
HNO3
SO4
SPM10(OBS)
200
150
100
50
0
3/1 0Z
3/2 12Z
3/4 0Z
3/4 12Z
3/7 0Z
3/8 12Z
3/10 0Z
3/13 0Z
3/16 0Z
3/19 0Z
3/22 0Z
3/25 0Z
3/28 0Z
3/31 0Z

Japan: 東京、大阪

Summary and concluding remarks

- Introduced two examples of wet deposition modeling;
- (1) Cloud-resolving
- (2) Non Cloud-resolving simplified approach
- (3) Further investigation of the cloud-resolving study may be necessary for improvement of wet deposition prediction; the research will also improve parameterization in the non cloud-resolving approach.

Summary and concluding remarks (continued)

- It may required such a model which can correctly reproduce mass balance of various chemical species in the atmosphere with keeping adequate accuracy for calculated concentration distributions of chemical species.

Transport/chemistry/deposition model for atmospheric trace chemical species

- An important tool:

  (1) for understanding of the effects of various human activities, such as fuel combustion and deforestation, on human health, eco-system, and climate, and

  (2) for planning of appropriate control of emission sources.

"Comprehensive" models such as RADM (Chang, et al., 1987); STEM-II (Carmichael, et al., 1986); CMAQ (Community Multiscale Air Quality model) by EPA for public use

- "Comprehensive" models include not only gas/aerosol phase chemistry but also aqueous phase chemistry in cloud/rain water in addition to the processes of advection, diffusion, wet deposition (mass transfer between aqueous and gas/aerosol phases), and dry deposition.